Critically coupled silicon Fabry-Perot photodetectors based on the internal photoemission effect at 1550 nm

Maurizio Casalino,* Giuseppe Coppola, Mario Iodice, Ivo Rendina, and Luigi Sirleto

Istituto per la Microelettronica e Microsistemi (IMM) - Consiglio Nazionale delle Ricerche – Sez. Napoli Italy
** maurizio.casalino@na.imm.cnr.it*

Abstract: In this paper, design, fabrication and characterization of an all-silicon photodetector (PD) at 1550 nm, have been reported. Our device is a surface-illuminated PD constituted by a Fabry-Perot microcavity incorporating a Cu/p-Si Schottky diode. Its absorption mechanism, based on the internal photoemission effect (IPE), has been enhanced by critical coupling condition. Our experimental findings prove a peak responsivity of 0.063 mA/W, which is the highest value obtained in a surface-illuminated IPE-based Si PD around 1550 nm. Finally, device capacitance measurements have been carried out demonstrating a capacitance < 5 pF which has the potential for GHz operation subject to a reduction of the series resistance of the ohmic contact.

OCIS codes: (040.0040) Detectors; (040.5160) Photodetectors; (040.6040) Silicon; (040.3060) Infrared; (250.0250) Optoelectronics; (260.5740) Resonance.

References and links

1. B. Jalali and S. Fathpour, "Silicon photonics," J. Lightwave Technol. **24**(12), 4600–4615 (2006).
2. L. K. Rowe, M. Elsey, N. G. Tarr, A. P. Knights, and E. Post, "CMOS-compatible optical rib waveguides defined by local oxidation of silicon," Electron. Lett. **43**(7), 392–393 (2007).
3. A. Liu, R. Jones, O. Cohen, D. Hak, and M. Paniccia, "Optical amplification and lasing by stimulated Raman scattering in silicon waveguides," J. Lightwave Technol. **24**(3), 1440–1455 (2006).
4. A. Liu, L. Liao, D. Rubin, H. Nguyen, B. Ciftcioglu, Y. Chetrit, N. Izhaky, and M. Paniccia, "High-speed optical modulation based on carrier depletion in a silicon waveguide," Opt. Express **15**(2), 660–668 (2007).
5. H. Park, Y. H. Kuo, A. W. Fang, R. Jones, O. Cohen, M. J. Paniccia, and J. E. Bowers, "A hybrid AlGaInAs-silicon evanescent preamplifier and photodetector," Opt. Express **15**(21), 13539–13546 (2007).
6. O. I. Dosunmu, D. D. Can, M. K. Emsley, L. C. Kimerling, and M. S. Unlu, "High-speed resonant cavity enhanced Ge photodetectors on reflecting Si substrates for 1550-nm operation," IEEE Photon. Technol. Lett. **17**(1), 175–177 (2005).
7. M. Casalino, G. Coppola, M. Iodice, I. Rendina, and L. Sirleto, "Near-infrared sub-bandgap all-silicon photodetectors: state of the art and perspectives," Sensors (Basel) **10**(12), 10571–10600 (2010).
8. T. K. Liang, H. K. Tsang, I. E. Day, J. Drake, A. P. Knights, and M. Asghari, "Silicon waveguide two-photon absorption detector at 1.5 μm wavelength for autocorrelation measurements," Appl. Phys. Lett. **81**(7), 1323–1325 (2002).
9. H. Chen, X. Luo, and A. W. Poon, "Cavity-enhanced photocurrent generation by 1.55μm wavelengths linear absorption in a p-i-n diode embedded silicon microring resonator," Appl. Phys. Lett. **95**(17), 171111 (2009).
10. M. W. Geis, S. J. Spector, M. E. Grein, R. T. Schulein, J. U. Yoon, D. M. Lennon, S. Deneault, F. Gan, F. X. Kaertner, and T. M. Lyszczarz, "CMOS-compatible all-Si high-speed waveguide photodiodes with responsivity in near-infrared communication band," IEEE Photon. Technol. Lett. **19**(3), 152–154 (2007).
11. M. W. Geis, S. J. Spector, M. E. Grein, J. U. Yoon, D. M. Lennon, and T. M. Lyszczarz, "Silicon waveguide infrared photodiodes with >35 GHz bandwidth and phototransistors with 50 AW-1 response," Opt. Express **17**(7), 5193–5204 (2009).
12. M. Casalino, L. Sirleto, L. Moretti, M. Gioffrè, G. Coppola, and I. Rendina, "Silicon resonant cavity enhanced photodetector based on the internal photoemission effect at 1.55 μm: Fabrication and characterization," Appl. Phys. Lett. **92**(25), 251104 (2008).
13. M. Casalino, L. Sirleto, L. Moretti, and I. Rendina, "A silicon compatible resonant cavity enhanced photodetector working at 1.55 μm," Semicond. Sci. Technol. **23**(7), 075001 (2008).
14. M. Casalino, L. Sirleto, M. Iodice, and G. Coppola, *Photodetectors* (InTech, 2012).

#162325 - $15.00 USD Received 31 Jan 2012; revised 13 Apr 2012; accepted 26 Apr 2012; published 18 May 2012

15. A. Akbari, R. N. Tait, and P. Berini, "Surface plasmon waveguide Schottky detector," Opt. Express **18**(8), 8505–8514 (2010).
16. W. F. Kosonocky, F. V. Shallcross, T. S. Villani, and J. V. Groppe, "160x244 Element PtSi Schottky-barrier IR-CCD image sensor," IEEE Trans. Electron. Dev. **32**(8), 1564–1573 (1985).
17. S. Zhu, M. B. Yu, G. Q. Lo, and D. L. Kwong, "Near-infrared waveguide-based nickel silicide Schottky-barrier photodetector for optical communications," Appl. Phys. Lett. **92**(8), 081103 (2008).
18. M. Casalino, L. Sirleto, M. Iodice, N. Saffioti, M. Gioffrè, I. Rendina, and G. Coppola, "Cu/p-Si Schottky barrier-based near infrared photodetector integrated with a silicon-on-insulator waveguide," Appl. Phys. Lett. **96**(24), 241112 (2010).
19. O. Mamezaki, M. Fujii, and S. Hayashi, "Internal photoemission from Ag nanoparticles embedded in Al_2O_3 film," Jpn. J. Appl. Phys. **40**(Part 1, No. 9A), 5389–5393 (2001).
20. I. Goykhman, B. Desiatov, J. Khurgin, J. Shappir, and U. Levy, "Locally oxidized silicon surface-plasmon Schottky detector for telecom regime," Nano Lett. **11**(6), 2219–2224 (2011).
21. J. Esper, P. Panetta, M. Ryschkewitsch, W. Wiscombe, and S. Neeck, "NASA-GSFC Nano-satellite technology for earth science missions," Acta Astronaut. **46**(2-6), 287–296 (2000).
22. C. Daffara, E. Pampaloni, L. Pezzati, M. Barucci, and R. Fontana, "Scanning multispectral IR reflectography SMIRR: an advanced tool for art diagnostics," Acc. Chem. Res. **43**(6), 847–856 (2010).
23. M. S. Ünlü and S. Strite, "Resonant cavity enhanced photonic devices," J. Appl. Phys. **78**(2), 607–639 (1995).
24. D. F. Logan, K. J. Murray, J. J. Ackert, P. Velha, M. Sorel, R. M. De La Rue, P. E. Jessop, and A. P. Knights, "Analysis of resonance enhancement in defect-mediated silicon micro-ring photodiodes operating at 1550 nm," J. Opt. A, Pure Appl. Opt. **13**, 125503 (2011).
25. M. Casalino, G. Coppola, M. Gioffrè, M. Iodice, L. Moretti, I. Rendina, and L. Sirleto, "Cavity enhanced internal photoemission effect in silicon photodiode for sub-bandgap detection," J. Lightwave Technol. **28**, 3266–3272 (2010).
26. H. C. Card, "Aluminum-silicon Schottky barriers and ohmic contacts in integrated circuits," IEEE Trans. Electron. Dev. **23**(6), 538–544 (1976).
27. D. A. G. Bruggeman, "Berechung verschiedener physikalischer Konstanten von heterogenen Substanzen. I. Dielektrizitatskonstanten und Leitfihigkeiten der Mischk6rper aus isotropen Substanzen," Ann. Phys. Leipzig **416**(7), 636–664 (1935).
28. P. I. Rovira, A. S. Ferlauto, J. Koh, C. R. Wronski, and R. W. Collins, "Optics of textured amorphous silicon surfaces," J. Non-Cryst. Solids **266–269**, 279–283 (2000).
29. M. Lončarić, J. Sancho-Parramon, and H. Zorc, "Optical properties of gold island films-a spectroscopic ellipsometry study," Thin Solid Films **519**(9), 2946–2950 (2011).
30. E. D. Palik, *Handbook of Optical Constants of Solids* (Academic Press, 1985).
31. R. H. Fowler, "The analysis of photoelectric sensitivity curves for clean metals at various temperatures," Phys. Rev. **38**(1), 45–56 (1931).
32. V. E. Vickers, "Model of schottky barrier hot-electron-mode photodetection," Appl. Opt. **10**(9), 2190–2192 (1971).
33. S. M. Sze, *Physics of Semiconductor Devices* (John Wiley & Sons, 1981).
34. G. T. Reed and A. P. Knights, *Silicon Photonics: An introduction* (John Wiley & Sons, 2005).
35. G. Coppola, A. Irace, A. Cutolo, and M. Iodice, "Effect of fabrication errors in channel waveguide Bragg gratings," Appl. Opt. **38**(9), 1752–1758 (1999).
36. S. S. Cohen, G. Gildenblat, M. Ghezzo, and D. M. Brown, "Al-0.9% Si/Si ohmic contacts to shallow junctions," J. Electrochem. Soc. **129**(6), 1335–1338 (1982).
37. A. Yariv, *Quantum Electronics* (John Wiley & Sons, 1989).
38. C. Scales and P. Berini, "Thin-film Schottky barrier photodetector models," IEEE J. Quantum Electron. **46**(5), 633–643 (2010).

1. Introduction

Silicon photonics offers the potential for low-cost integration of optical and electronic functionality on the same chip providing a remarkable impact on many sectors such as telecommunications, optoelectronics and microelectronics [1]. Indeed, the fabrication of silicon-based optical devices could be able to utilize the enormous infrastructures well developed in the years of the strong microelectronics industry growth. In the past two decades certain important developments, including the demonstration of high-Q resonators, high-speed modulators, couplers, and optically pumped lasers, based on silicon substrate have been achieved [2–4].

Photodetectors are key components in all-silicon photonic systems. Though Silicon (Si) optical detectors have already found wide acceptance for visible light (0.400-0.700 μm), at the wavelength of interest for telecommunications (2° and 3° window), due to their cut-off wavelength of about 1.1 μm, they are not the most promising. An interesting approach is the

#162325 - $15.00 USD Received 31 Jan 2012; revised 13 Apr 2012; accepted 26 Apr 2012; published 18 May 2012

hybrid integration of exotic material based detectors with Si optical circuits [5,6]; however a truly monolithic fabrication technology is still preferred [7]. Therefore, in the last years, in order to take advantage of low-cost standard Si-technology, a number of options have been proposed: two-photons absorption [8]; the incorporation of optical dopants/defects with midbandgap energy levels into the Si lattice [9–11]; internal photoemission effect (IPE) [12–14], recently adopted in silicon photodetectors based on surface plasmons [15], too.

IPE occurs in a Schottky structure when hot carriers, generated in the metal by the absorption of photons, gain sufficient energy to overcome the Schottky barrier and to be collected as photocurrent. This mechanism allows sub-bandgap detection and Si infrared photodiodes based on IPE are usually employed in the infrared imaging systems [16]. The main advantages of these devices resides in their extremely large bandwidth and simple fabrication process, but unfortunately, their quantum efficiency is very low. An improvement in efficiency is generally achieved by lowering the potential barrier, unfortunately, due to the increased dark current, such devices have to work at cryogenic temperature. In order to get reasonable responsivity the principal challenge consists of uncovering new device architectures and designs allowing their use at room temperature. Interestingly, devices based on IPE encompasse both micro- and nano-photonics structures. The former is generally based on the merging of Schottky diodes with a dielectric waveguide [17,18], the latter refers to plasmonic effects in thin metal film and metal nanoparticles [15,19–20]. In recent years, responsivity of IPE-based PDs has increased becoming adapted for power monitoring applications and resulting very promising in the telecommunications field. It is worth noting that IPE-based waveguide PDs are inherently more responsive than IPE-based surface-illuminated PDs because optical power can be confined at the metal-semiconductor interface; for this reason many efforts have been focused on waveguide structures [15,17–18] and only few investigations have been carried out on surface-illuminated devices. On the other hand, waveguide structures are not suitable in some cases where surface-illuminated devices are the only option; for instance, in imaging applications where the vision can be improved in critical conditions such as smoke and fog thanks to reduced scattering at NIR wavelengths [21] or in reflectography applications where the transparency of most pigments to NIR wavelengths are used to investigate ancient paintings [22].

PD performance can be increased by resonant cavity enhanced (RCE) structures, which have been extensively investigated in literature [23] showing their capability of provide near unity efficiency without hampering bandwidth upon critical coupling (CC) condition [23–26]. In our previous paper [25], we investigated RCE IPE-based back-illuminated PDs proving that their responsivity could be enhanced by increasing the optical field inside a Fabry-Perot microcavity. It is worth noting that our structure is different from the classical RCE Schottky PDs [6] where the Schottky metal acts only as cavity mirror, while in our device the metal layer acts both as active (absorbing) layer and as cavity mirror.

In this paper, we investigate the possibility to extend RCE PDs CC theory in order to maximize responsivity of the proposed device. Our findings confirm that critically coupled devices show an increase in responsivity with respect to not critically coupled device [25], becoming very appealing for the aforementioned applications. Finally, measured device capacitance demonstrates the potential for GHz operation subject to a reduction of the series resistance of the ohmic contact.

2. Fabrication and materials

The sketch of the device is shown in Fig. 1. Proposed PD is a vertically illuminated Fabry-Perot structure formed by a bottom distributed Bragg reflector (DBR), a top thick metal reflector and, in the middle, a silicon cavity [25]. It is worth noting that top thick metal reflector works as cavity mirror and active absorbing layer at the same time.

#162325 - $15.00 USD Received 31 Jan 2012; revised 13 Apr 2012; accepted 26 Apr 2012; published 18 May 2012

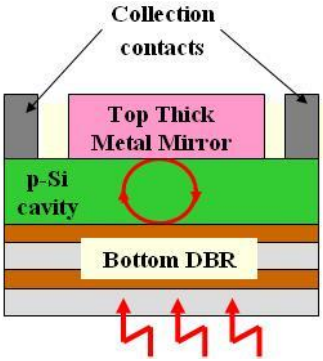

Fig. 1. Schematic cross section of the proposed photodetector.

The samples were fabricated starting from a slightly doped (10^{14} cm^{-3}) p-type bi-polished 100-µm-thick silicon wafer. On the back, a multilayer Bragg mirror is fabricated by Plasma Enhanced Chemical Vapor Deposition (PECVD) technique. The mirror is composed by a quarter-wave stack of a–Si:H and Si_3N_4 layers, having nominal refractive index, at 1550 nm, of 3.52 and 1.82, respectively. The reflector is realized with periods of a–Si:H/Si_3N_4 pairs, whose nominal thicknesses are 110 nm and 213 nm, respectively. Silicon nitride is deposited at pressure of 1.2 mbar, temperature of 250 °C, at 30 W of RF power. In the deposition chamber 10 sccm of NH_3, 88 sccm of SiH_4 (5% in He) and 632 sccm of N_2 are flowed. The deposition rate is 22.93 nm/min and the suited Si_3N_4 thickness is obtained with a process time of 9 min and 17 sec. Amorphous hydrogenated silicon, instead, is deposited at pressure of 0.8 mbar, temperature of 250°C, power of 2W and a SiH_4 (5% in He) flow of 600 sccm. The a-Si:H deposition rate is 3.15 nm/min and the desired thickness is obtained with a process time of 34 min and 56 sec.

The collecting ohmic contact and the Schottky contact were both realized on the top of the sample. The collecting contact was made by a 200-nm-thick aluminum (Al) film, thermally evaporated at $3 \cdot 10^{-6}$ mbar and 150 °C, patterned by a lift-off process of photoresist Shipley S1813 which, deposited by a spin-coater at 4000rpm, has a thickness of 1.4 µm. Then an annealing at 475 °C in nitrogen for 30 min, in order to get a not-rectifying behavior, was carried out [26]. Finally, the Schottky contact was fabricated. Copper (Cu) was thermally evaporated and patterned by lift-off, so obtaining a thickness of 200 nm, thicker than optical field penetration depth. The collecting contact and the Schottky contact are shaped as a Schottky metal disk placed inside an ohmic metal ring (Fig. 2). Two series of devices with radius of 40 µm and 20 µm, respectively, have been realized. The distance between the edge of the Schottky and ohmic contact is about 2 µm.

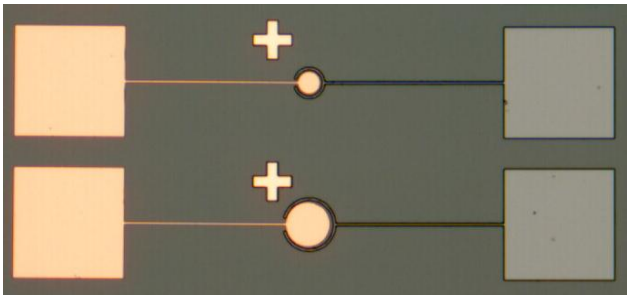

Fig. 2. Top view of the proposed fabricated devices.

In order to accommodate more accurate simulations, the optical properties of all used materials (Cu, a-Si:H and Si_3N_4) for the device fabrication are measured by ellipsometric

#162325 - $15.00 USD Received 31 Jan 2012; revised 13 Apr 2012; accepted 26 Apr 2012; published 18 May 2012

analysis. The optical functions of Cu film were determined using a model obtained from a superposition of a Lorentz dielectric function and the Drude model. Moreover, ellipsometric analysis was used to derive the surface roughness of Cu film. The Cu film surface roughness was modeled as a 50/50 vol% mixture of Cu layer refractive index and voids, applying the Bruggeman Effective Medium Theory (EMT) model [27–28]. The estimated surface roughness thickness was approximately 2 nm. The fitting of experimental data returned a goodness of fit (GOF) parameter $\chi^2 = 0.26$, defined as reported in Ref. [29].

In Fig. 3 we have plotted real and imaginary parts of the refractive index of Cu in the whole spectral range 280-1600 nm, compared with dispersion spectra for *n* and *k* reported by E. D. Palik [30], limited to 1200 nm.

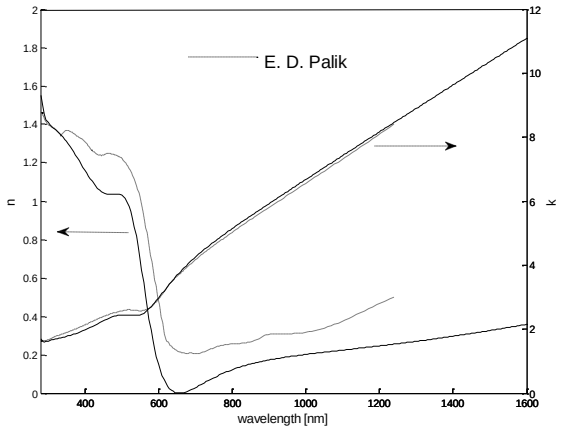

Fig. 3. Cu complex refractive index dispersion.

As reported in Table 1, refractive index real part and extinction coefficient at 1550 nm, are 0.397 and 10.72, respectively.

Moving our attention on Bragg mirror optical properties, the determination of its refractive index, extinction coefficient and thicknesses of a–Si:H and Si_3N_4 layers, has been reported in our previous work [25], while their values are summarized in Table 1.

Table 1. Value of Thickness and Complex Refractive Index at 1550nm as Calculated

	Thickness [nm]	$n_{@1550}$
Cu	200	0.397 – j 10.72
a–Si:H	108	3.58
Si_3N_4	220	1.82

3 Design: analytical model and results

It is well-known that responsivity of IPE-based devices can be written as [13]:

$$\mathrm{Resp} = \frac{\lambda[\mathrm{nm}]}{1242}\eta = \frac{\lambda[\mathrm{nm}]}{1242}A_T F_e P_e \eta_c \qquad (1)$$

where λ is the wavelength, η is the external quantum efficiency, A_T is the total metal optical absorbance [13], F_e is the fraction of absorbed photons which produce photoelectrons with appropriate energy to contribute to the photocurrent [31], F_e is depending on the height of the Schottky barrier Φ_{B0} as shown in Fig. 4(a), P_E is the total accumulated probability that one of these photoexcited electrons will overcome the Schottky barrier after scattering with cold electrons and/or boundary surfaces [32] (depending on the metal thickness), and η_c is the

#162325 - $15.00 USD Received 31 Jan 2012; revised 13 Apr 2012; accepted 26 Apr 2012; published 18 May 2012

barrier collection efficiency, which depends on the applied voltage, due to the image force effect [33] which causes a potential barrier lowering ($\Delta\Phi_B$) and a displacement (x_m), as shown in Fig. 4(a). While F_e, P_e and η_c have an analytical formulation [13], this is not true for A_T in IPE-based optical cavity structures. The cavity plays a key role in the calculation of the A_T factor which, generally, is carried out by using the transfer matrix method (TMM) [13]. In this section, we propose a very simple analytical model, derived from the theory of the Fabry-Perot resonator, in order to calculate A_T and to verify that CC condition theory can be extended to proposed device.

As shown in Fig. 4(b), our device can be schematized as an asymmetric plane mirrors Fabry-Perot interferometer where the input and output mirrors are a DBR and a silicon/metal interface, respectively. It is worth noting that the metal is approximated as semi-infinite because its thickness is considered greater than light penetration depth (δ) at wavelengths of interest.

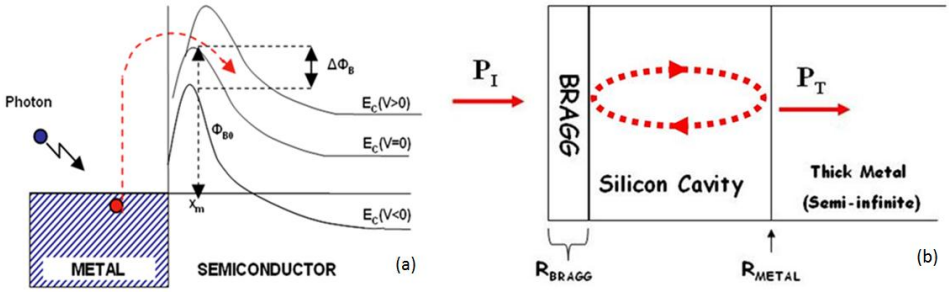

Fig. 4. (a) Energy band diagram for a metal/n-semiconductor junction. (b) Schematization of the proposed device as an asymmetric plane mirror Fabry-Perot resonator.

By the well-known Airy's formula, the optical intensity (P_T) transmitted through such a cavity is related to the incident light intensity P_{inc} by [34]:

$$\frac{P_T}{P_{inc}} = \frac{(1-R_{DBR})(1-R_{METAL})e^{-\gamma L}}{\left(1-\sqrt{R_{DBR}R_{METAL}}e^{-\gamma L}\right)^2 + 4\sqrt{R_{DBR}R_{METAL}}e^{-\gamma L}sen^2\frac{\phi}{2}} \tag{2}$$

where R_{DBR} and R_{METAL} are input and output mirror reflectivity, respectively, L is the silicon cavity length, γ is the round-trip loss coefficient and ϕ is the phase difference between successive waves in the cavity. If the metal thickness can be considered semi-infinite, all the transmitted power P_T will be absorbed and the Airy's formula describes the metal absorbance $A_T = P_T/P_{inc}$.

By these considerations the absorbance A_T can be maximized by maximizing the peak trasmittivity through the Fabry-Perot micorcavity, i.e., by fulfilling the following conditions:

- $$\phi = 2m\pi \qquad (m = 0,1,2,...) \tag{3}$$
- $$R_{DBR} = R_{METAL}e^{-2\gamma L} \tag{4}$$

When only condition (3) is fulfilled, i.e., at resonance wavelengths, absorbance can be written as:

$$A_T^{RES} = \frac{(1-R_{DBR})(1-R_{METAL})e^{-\gamma L}}{\left(1-\sqrt{R_{DBR}R_{METAL}}e^{-\gamma L}\right)^2} \tag{5}$$

However, this absorbance is not the maximum, because it occurs when also condition (4) is fulfilled, i.e., when the output mirror reflectivity is properly linked to the output mirror reflectivity:

#162325 - $15.00 USD Received 31 Jan 2012; revised 13 Apr 2012; accepted 26 Apr 2012; published 18 May 2012

$$\left(A_T^{RES}\right)_{MAX} = \frac{(1-R_{METAL})e^{-\gamma L}}{(1-R_{METAL}e^{-2\gamma L})} \tag{6}$$

It is worth noting that if the round-trip loss coefficient can be neglected ($\gamma \approx 0$) an absorbance of 1 is obtained when Eq. (3) and Eq. (4) are contemporaneously fulfilled.

By means of the measured dispersion curves, accurate simulations, in order to design an optimized device, have been carried out. In Fig. 5 DBR reflectivity at 1550 nm plotted against number of stacks of a-Si:H/Si_3N_4, is reported, in addition reflectivity of 200 nm-thick-Cu metal mirror at 1550 nm is reported, too.

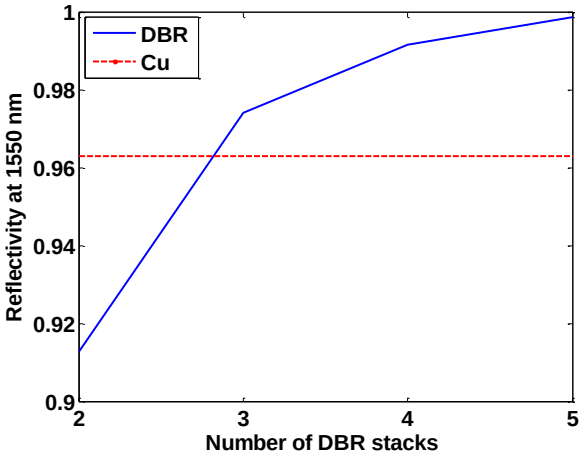

Fig. 5. Reflectivity versus number of DBR stacks at 1550 nm (blue solid line). Horizontal line is 200 nm-thick-Cu mirror reflectivity at 1550 nm (red dashed line).

Figure 5 shows that around 1550 nm, DBR reflectivity can approach metal reflectivity if DBR is constituted by 3 pairs of a-Si:H/Si_3N_4. At resonance wavelengths, as shown above, this is the best option in order to get a further increase in responsivity when small round-trip losses are considered. This can be also shown in Fig. 6 where absorbance at resonance wavelength for a 200 nm-thick-Cu metal mirror (reflectivity of 0.964) is plotted against DBR reflectivity. Figure 6 can be derived by Eq. (5) but in order to validate the proposed analytical model, it was calculated also by a numerical method (TMM) resulting in a good agreement. Figure 6 shows that with a right choice of the DBR reflectivity a further increase in absorbance (i.e., in responsivity) can be obtained. In fact, as can be view in Fig. 6, when DBR is formed by 5 pairs of a-Si:H/Si_3N_4 absorbance dramatically decreases lowering device responsivity [25]. A fine-tuning of DBR reflectivity can fulfill an ultimate optimization of the cavity, with the aim to get the maximum value of absorbance. In order to obtain a value of DBR reflectivity that perfectly matches the Cu mirror one, it is possible to detune the resonance of dielectric mirror during its fabrication. In particular, the realization of dielectric layers whose thickness is deliberately different from the nominal value of $\lambda/4n$ allows to predetermine the DBR reflectivity [35] and get the perfect matching with the metallic mirror value.

#162325 - $15.00 USD Received 31 Jan 2012; revised 13 Apr 2012; accepted 26 Apr 2012; published 18 May 2012

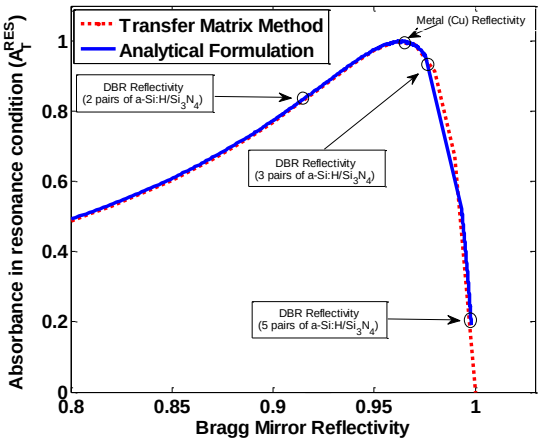

Fig. 6. Proposed device simulated absorbance in resonance condition vs DBR reflectivity.

4. Characterization

The fabricated devices have been characterized in terms of J-V electrical characteristic, responsivity and junction capacitance.

4.1. Schottky barrier height measurements

Typical density current-voltage (J-V) curve of Cu/p-Si diodes, experimentally obtained by a parameter analyzer (Hewlett Packard 4145B), is depicted in Fig. 7.

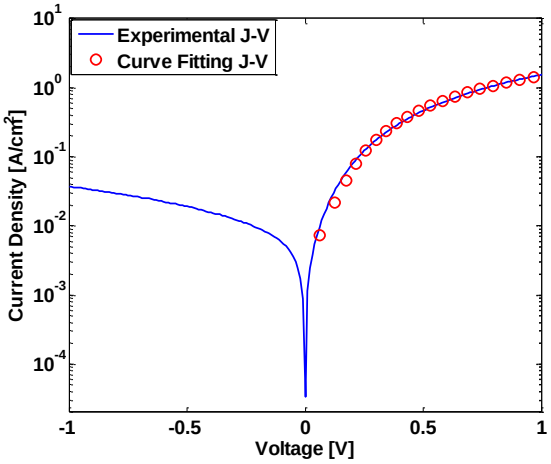

Fig. 7. J-V characteristic and respective curve fitting of the proposed device.

The Schottky barrier height (SBH) is deduced fitting the experimental J-V characteristic in the forward bias region by the canonical equation of the Schottky diode [33]. The calculated SBH and series resistance are 0.55 eV and 7 kΩ, respectively. High series resistance is due to a slight rectifying effect of the aluminium electrode realized on top of lightly doped p-type silicon.

4.2 Responsivity measurements

Experimental set-up has been already described in detail in our previous work [25]. Responsivity measurements carried out on the device having a Schottky Cu disk with radius

#162325 - $15.00 USD Received 31 Jan 2012; revised 13 Apr 2012; accepted 26 Apr 2012; published 18 May 2012

of 40 µm, into the range of 1545-1554 nm (step of 0.01 nm) at 100 mV of reverse bias applied, are reported in Fig. 8. Measured peak responsivity, finesse and free spectral range (FSR) are of about 55 µA/W, 14.5 and 3.3 nm, respectively.

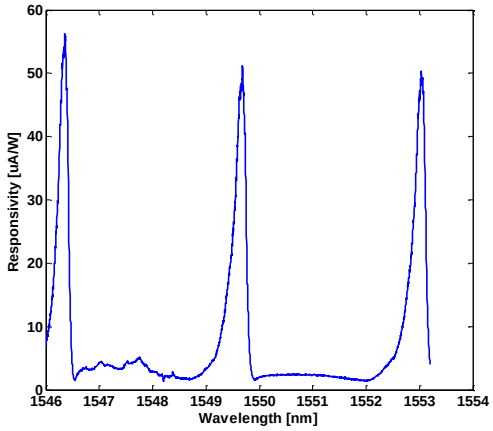

Fig. 8. Measured responsivity versus wavelength for the proposed for the proposed 40 µm-radius-photodetector.

It could be worth noting that as the responsivity is increased, the finesse is decreased with respect to results reported in Ref. 25 (8 µA/W and 33, respectively). This is an obvious consequence of the optimization process driving towards the fabrication of less reflective DBR lowering the resultant finesse.

In Fig. 9 measurements carried out on the device having a Schottky Cu disk with radius of 20 µm, into the range of 1545-1554 nm (step of 0.01 nm) at 100 mV of reverse bias applied, are reported. Also if FSR and finesse remain substantially the same, in this case responsivity slightly increases probably due to the increasing of the collection efficiency associated to the smaller path carriers.

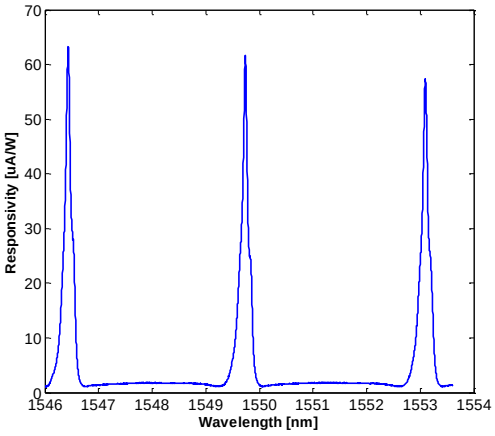

Fig. 9. Measured responsivity versus wavelength for the proposed 20 µm-radius-photodetector.

In our knowledge, a peak responsivity of 0.063 mA/W is the highest value obtained in a surface-illuminated IPE-based Si PD around 1550 nm.

#162325 - $15.00 USD Received 31 Jan 2012; revised 13 Apr 2012; accepted 26 Apr 2012; published 18 May 2012

4.3 Capacitance measurements and estimated bandwidth

The electrical properties of diodes based on Schottky junctions are determined by majority carrier phenomena, while for p-n diodes they are primarily determined by minority carriers. Therefore, the Schottky diodes can be switched faster because there are no minority carrier storage effects. It is well known that the response time of Schottky device is primarily determined by the electrical frequency response or RC time required to discharge the associated capacitance (C) through the resistance (R_s):

$$f_{3dB} = \frac{1}{2\pi R_s C} \tag{7}$$

Bandwidth estimation can be carried out by extracting R_s from the experimental J-V electrical characteristic and measuring C by a LCZ meter (Keithley-3322) which drives the device with a known AC voltage input signal deriving the capacitance by precisely measuring the resultant current. We used this approach in our previous work on the proposed device with radius of 40 μm obtaining a minimum capacitance value of 3 pF [25]. At the same way, capacitance measurement on the proposed 20 μm-radius-device is reported in Fig. 10 and shows a value of 1.6 ± 0.2 pF starting from a reverse bias of 2 V.

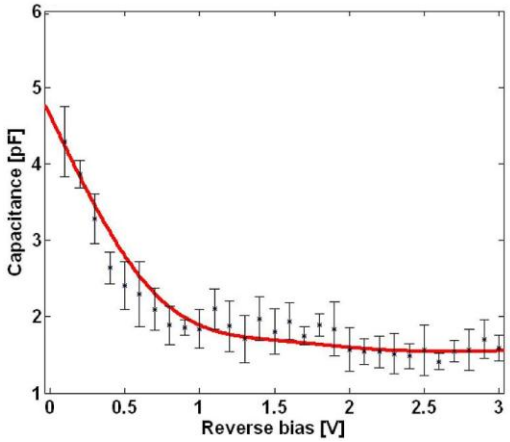

Fig. 10. Measured junction capacitance vs reverse bias for the proposed 20 μm-radius-device.

Unfortunately, the series resistance R_s = 7 kΩ (see sec. 4.1) is rather large due to the not-rectifying contact realized without a heavily P-doped region under the contact. For this reason, the estimated device bandwidth is limited to MHz range but could be easily improved toward GHz operation in an optimized device provided of a good ohmic contact. The general technique for making a satisfactory ohmic contact involves the establishment of a heavily doped (N^+ or P^+) surface layer on which an alloy of Al-Si is deposited (not pure Al is used in order to prevent diffusion of Si into Al). Specific contact resistance of an alloy Al-0.9% Si deposited on P^+ doped Si (surface dopant concentration of $6 \times 10^{19} cm^{-3}$) is about 15 Ω·μm^2 [36]. This value allows to get contact resistance < 1 Ω, when the metal contact area is larger than 15 μm^2. In this case, by considering the lowest measured capacitance of 1.6 pF reported in Fig. 10, a constant time τ < 1.6 ps could be obtained, enabling bandwidth greater than 99 GHz for an optimized devices not subject to others dynamic limitations. In fact, in order to obtain a complete evaluation of the proposed device bandwidth, two important limiting factors have to be considered: the the photon lifetime and the transit time.

The photon lifetime (τ_p) can be viewed as the time required to build or decay the optical field distribution inside the cavity and is given by [37]:

#162325 - $15.00 USD Received 31 Jan 2012; revised 13 Apr 2012; accepted 26 Apr 2012; published 18 May 2012

$$\tau_p = \frac{Q}{2\pi c}\ \lambda \tag{8}$$

where Q is the quality factor of the resonator and c is the vacuum light speed. For a Q of 6800 extracted from Fig. 9 and at 1550 nm, τ_p is 5.6 ps which is much smaller than estimated drift time τ_{tr} of 220 ps required for carriers generated in the centre of the Schottky metal disk to reach the ohmic contact (depletion width of 22 μm and saturation velocity of 10^7 cm/s [33]).

5. Conclusions

In this paper, design, fabrication and characterization of a critically coupled IPE-based surface-illuminated Si PDs at 1550 nm, have been reported. We have proved, both theoretically and experimentally, that a significant increase in responsivity is obtained taking advantage of critical coupling condition.

Devices exhibit a maximum responsivity of 0.063 mA/W around 1550 nm. Measured responsivity is the highest value reported in literature concerning a surface-illuminated IPE-based Si PD at 1550 nm and these devices result attractive for power monitoring, imaging and reflectography NIR applications. Moreover, junction capacitance measurements (pF) encourage pursuing increased bandwidth toward several GHz operation. The main advantages of IPE-based PDs reside in their extremely large bandwidth (unipolar devices) and simple fabrication process.

Finally device performances could be further improved: concerning bandwidth is mandatory to improve the ohmic contacts quality to get a lower series resistance, concerning responsivity could be useful to make thinner Schottky metal in order to take advantage from the internal photoemission increase due to improved carriers escape probability through the Schottky barrier [38].

#162325 - $15.00 USD Received 31 Jan 2012; revised 13 Apr 2012; accepted 26 Apr 2012; published 18 May 2012